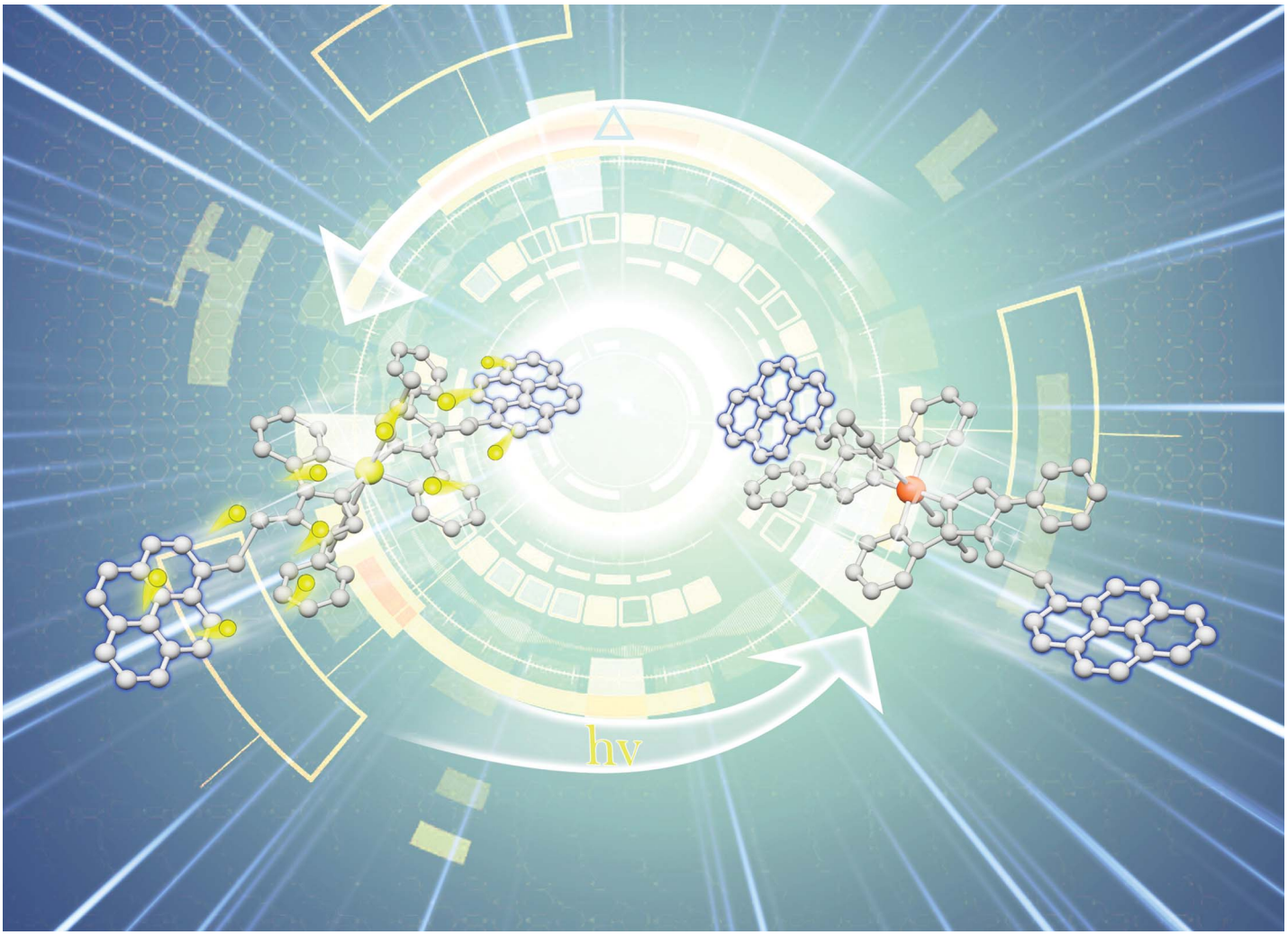

Showcasing research from Professor Tao Liu's laboratory, School of Chemistry, Dalian University of Technology, Dalian, China.

Fluorescence modulation *via* photoinduced spin crossover switched energy transfer from fluorophores to Fe^{II} ions

A mononuclear compound was constructed *via* the coordination of fluorophores with Fe^{II} ions, whose electronic configuration changed from low spin to high spin upon light irradiation. The effective spectral overlap between the emission of the fluorophores and the absorption band of the Fe^{II} ions differed between the low spin and high spin states. The photoinduced spin-crossover switched the energy transfer from the fluorophore to the Fe^{II} ion, resulting in a 20% increase in fluorescence emission intensity. The presented results provide a novel approach for developing optical memory and sensors *via* photoinduced electron rearrangement.

As featured in:

Tao Liu *et al.*, *Chem. Sci.*, 2018, **9**, 2892.

ROYAL SOCIETY OF CHEMISTRY

rsc.li/chemical-science

Registered charity number: 207890

Chemical Science

EDGE ARTICLE

View Article Online
View Journal | View Issue

Cite this: *Chem. Sci.*, 2018, **9**, 2892

Fluorescence modulation *via* photoinduced spin crossover switched energy transfer from fluorophores to Fe^{II} ions†

Jun-Li Wang,[a] Qiang Liu,[a] Yin-Shan Meng,[a] Xin Liu,[a] Hui Zheng,[b] Quan Shi,[b] Chun-Ying Duan[a] and Tao Liu*[a]

Molecular materials possessing phototunable fluorescence properties have attracted great interest owing to their potential applications in optical switches and storage. However, most fluorescence modulation is realized through light-responsive structural isomerization in solution. It is a formidable challenge to achieve phototunable fluorescence emission with high fatigue resistance and a fast response rate in the solid state for the development of devices. Here, a mononuclear compound was constructed *via* the coordination of fluorophores with Fe^{II} ions, whose electronic configuration changed from low spin to high spin upon light irradiation. The photoinduced spin crossover of Fe^{II} ions was accompanied by a 20% increase in the fluorescence emission intensity. A temperature-dependent spectroscopic study together with time-dependent density functional theory calculations revealed that the effective spectral overlap between the emission of the fluorophores and the absorption band of the Fe^{II} ions differed between the low spin and high spin states. The photoinduced spin crossover switched the energy transfer from the fluorophore to the Fe^{II} ion, resulting in fluorescence modulation. The presented results provide a novel approach for developing optical memory and sensors *via* electron rearrangement of photoinduced spin crossover.

Received 9th December 2017
Accepted 2nd February 2018

DOI: 10.1039/c7sc05221a

rsc.li/chemical-science

Introduction

The application of fluorescent materials for detection and tracer techniques is highly desirable because fluorescence signals provide superior contrast and sensitivity during remote detection at relatively high spatial and temporal resolution.[1,2] The modulation of fluorescence signals *via* light is particularly attractive for noninvasive optical read-out technologies owing to the potential applications in optical storage, optical switches and sensors.[3–7] Producing a coupling between a fluorophore unit and a light-responsive unit is a rational way to yield photoswitchable fluorescence emission. Previous strategies for achieving phototunable fluorescence emission for the development of new fluorescence switches mainly involved linking organic photochromic groups with fluorescent units *via* covalent bonds.[7–12] Within the large family of photochromic groups, most are based on the photoisomerization of organic molecules, such as *cis*/*trans* or opened/closed ring isomerization.[13–19] The fluorescence emission is modulated as a result of changes in the intramolecular energy transfer and/or electron transfer from the fluorescent donor to the photochromic acceptor during the process of a photochemical reaction under alternating ultraviolet and visible light irradiation.[20] However, photoisomerization often results in the drastic movement of atoms, which are strongly restricted in the solid state due to tension and hindrance. Therefore, efficient photoisomerization reactions commonly occur in solution rather than the solid state. It is challenging to realize phototunable fluorescence in the solid state and thus develop applicable devices with high fatigue resistance and a fast response rate.

When compared with the photoisomerization of organic molecules, the photoswitchable electron rearrangement of metal ions, such as spin crossover (SCO) and electron transfer, has been realized in the solid state with a fast response rate and good reversibility, accompanied by drastic changes in the electronic and crystal structure of the materials.[21–23] Such drastic changes should sufficiently perturb the environment of the fluorophore and further allow a fluorescent response;[24–34] thus providing a promising candidate for a light-responsive unit with which to construct photoswitchable fluorescent molecular devices. However, two challenges remain in achieving the goal in this system. One is how to preserve both the fluorescent function and the photoinduced electron rearrangement

[a]*State Key Laboratory of Fine Chemicals, Dalian University of Technology, 2 Linggong Rd., 116024, Dalian, China. E-mail: liutao@dlut.edu.cn*

[b]*Thermochemistry Laboratory, Liaoning Province Key Laboratory of Thermochemistry for Energy and Materials, Dalian National Laboratory for Clean Energy, Dalian Institute of Chemical Physics, Chinese Academy of Sciences, Dalian 116023, China*

† Electronic supplementary information (ESI) available: Synthesis and physical measurement details. Crystal data in CIF format and additional figures (Fig. S1–S14). CCDC 1447594 and 1447595. For ESI and crystallographic data in CIF or other electronic format see DOI: 10.1039/c7sc05221a

phenomenon when combining them in a single component because both are highly sensitive to minor external physical and internal chemical changes. The other is how to build an effective coupling pathway to realize the synergy between them, thereby obtaining photoswitchable fluorescence emission.

Photoinduced SCO of Fe^{II} ions is a typical example of photoswitchable electron rearrangement,[35–41] which could serve as a light-responsive unit for coupling with an organic fluorophore unit *via* a coordination bond linkage. To retain fluorescence and SCO behavior, the fluorescent ligand should exhibit sufficiently strong fluorescence emission and overcome the quenching effect when coordinated with Fe^{II} ions. Meanwhile, the Fe^{II} ions must be located within a suitable ligand field to support the spin transition triggered by light. Moreover, to achieve synergy, the emission or excitation band of the ligand should have an effective spectral overlap with the absorption band of the Fe^{II} ions at a given spin state. Considering the above, we designed a fluorophore ligand (pyrene-1-yl)-*N*-(3,5-di(pyridin-2-yl)-4*H*-1,2,4-triazol-4-yl)methanimine (L). This ligand shows strong fluorescence emission at 516 nm, thus overlapping with the typical absorption region of Fe^{II} complexes.[38] Therefore, the fluorescence emission is expected to be quenched or increased depending on whether the resonant energy transfer from the fluorescent donor to the Fe^{II} acceptor occurs in the photoinduced spin transition process (Scheme 1). According to this strategy, we successfully obtained a mononuclear complex $[Fe(L)_2(NCS)_2]$ (**1**), which exhibited significant enhancement in both fluorescence emission intensity and magnetization upon light irradiation at 671 nm. These findings provide direct evidence for photoswitchable fluorescence emission *via* photoinduced electron rearrangement in a fluorescence-coupled SCO complex.

Results and discussion

Green crystals of **1** were obtained by the diffusion of diethyl ether into a DMF solution of **1**. Complex **1** was crystallized in the triclinic space group $P\bar{1}$. The iron(II) ion adopted an N_6 octahedral coordination configuration, surrounded by two nitrogen atoms from two *trans*-isothiocyanate anions and four nitrogen atoms from two bidentate ligands (Fig. 1). The solvent-free complex **1** showed high thermal stability up to 200 °C (Fig. S1†). At 277 K, the Fe–$N_{pyridyl}$ bond length (2.197(2) Å) was slightly longer than the Fe–$N_{triazole}$ (2.124(2) Å) and Fe–$N_{isothiocyanate}$ (2.077(3) Å) bond lengths, which were close to that of Fe_{HS}^{II}–N (HS = high spin).[42] The bond lengths were in the range of 2.014(2)–1.932(2) Å at 90 K (Table S3†), which is in agreement with related Fe_{LS}^{II} (LS = low spin) complexes containing bidentate abpt ligands.[43,44] These temperature-dependent structural variations suggest the occurrence of thermal-induced SCO. The spin transition from HS to LS was also verified by the change in the distortion of the N_6 octahedron. The Σ parameter, defined as the total deviation of the 12 *cis* N–Fe–N angles from 90°, decreased from 72° to 51° when samples were cooled from 277 to 90 K. When compared with the HS state structure, the LS state structure showed a smaller deformation. This phenomenon is consistent with that previously observed in other SCO complexes.[45–47]

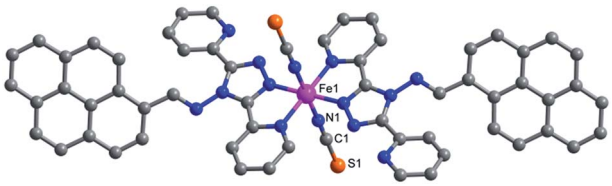

Fig. 1 The crystal structure of complex **1**. The pink, gray, blue and orange spheres represent Fe^{II}, C, N and S atoms, respectively. Hydrogen atoms are omitted for clarity.

Adjacent molecules were connected *via* π···π stacking interactions involving pyridine rings to form a one-dimensional (1D) supramolecular chain along the crystallographic *b* axis. At 277 K, the π···π interactions are characterized by a centroid-to-centroid distance of 3.91 Å. Such one-dimensional chains are associated through four face-to-face π···π interactions between pyrene rings generating a 3D supramolecular network. The centroid-to-centroid distances are 3.66 Å, 3.86 Å and 3.85 Å (Fig. S2†).

To confirm the photo-responsive properties of the SCO unit, the magnetic susceptibilities of **1** were measured before and after irradiation. The temperature-dependent magnetic measurement revealed that complex **1** underwent complete SCO with a transition temperature ($T_{1/2}$) of 267 K (Fig. S4†). As the temperature increased from 2 K after irradiation at 671 nm, the χT value increased from 0.05 $cm^3\ mol^{-1}$ K to a maximum value of 0.68 $cm^3\ mol^{-1}$ K at 12 K due to the light-induced excited spin state trapping (LIESST) effect, and this corresponds to the trapping of approximately 21.3% of the metastable Fe_{HS}^{II} ions (Fig. S5†). Moreover, the irradiation-time dependence of the infrared (IR) spectra further verifies the trapping of the photogenerated metastable Fe_{HS}^{II} ions by irradiation at 20 K. The ν_{NCS^-} stretching bands (2080 cm^{-1}) in the HS state began to appear after irradiation at 671 nm for 10 min and the intensity of the HS mode increased with increasing irradiation time (Fig. S6†). This result can be attributed to the photoinduced spin transition from the LS state to the metastable HS state. The photogenerated magnetization relaxed to the initial value upon heating to 60 K. Relaxation of the photoinduced metastable state was monitored at 10 K to probe the stability of the photoinduced phase, which can be determined based on the time decay of the magnetization after irradiation (Fig. S7†). The photoinduced phase showed considerable stability with

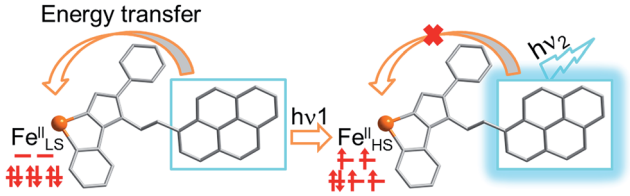

Scheme 1 Modulation of fluorescence emission *via* energy transfer with a photoinduced spin transition from Fe_{LS}^{II} to Fe_{HS}^{II}.

a relaxation time of 3331.75 s at 10 K, which was sufficiently long to monitor the phototunable fluorescence emission at 10 K.

To verify the fluorescent properties, the fluorescence emission spectra of **1** and the ligand were obtained. At room temperature, ligand L showed an emission band at 516 nm under excitation at 380 nm (Fig. S8†). At the same excitation wavelength, the fluorescence emission spectrum of **1** displayed a maximum emission at 513 nm at 300 K, indicating that the fluorescence property of the ligand was well retained when coordinated with Fe_{HS}^{II} ions. The fluorescence emission of **1** before and after irradiation was recorded to further examine the photoswitchable fluorescence emission behavior at 10 K. Interestingly, a significant increase in fluorescence emission intensity was observed after 2 h of irradiation. The increased degree (ΔR) before and after irradiation is defined as $\Delta R = (R_1 - R_0)/R_0$, where R_0 and R_1 are the emission intensities before and after 2 h of irradiation at 498 nm, respectively. The ΔR value of complex **1** reached up to 19.8% at 10 K, which is in agreement with the increased degree of magnetic susceptibility before and after irradiation. Thus, the above results demonstrate that fluorescence emission intensity can be controlled by photoinduced SCO from Fe_{LS}^{II} to Fe_{HS}^{II} ions. The fluorescence emission intensity of the photogenerated metastable state decayed rapidly upon heating (Fig. 2), which is consistent with the temperature-dependent magnetization behavior of the photogenerated metastable state. When the temperature was increased to 40 K, the emission spectrum almost overlapped with that obtained before irradiation at 10 K, demonstrating that the emission intensity of **1** could be increased by light irradiation and decreased by thermal treatment. This increase is possibly related to a photoinduced spin transition from the LS state to the HS state of Fe^{II} ions, whereas the decrease was caused by thermal relaxation of the photogenerated metastable HS state.

The correlation between the fluorescence and the spin state of the Fe^{II} ions was studied to verify the photoinduced SCO tuning of the fluorescence emission intensity. As mentioned earlier, complex **1** was in the HS state at room temperature and the LS state at 90 K. With a temperature decrease from 300 to 200 K, the χT value decreased abruptly from 2.78 to 0.20 cm^3 mol^{-1} K, gradually reaching a minimum value of 0.08 cm^3 mol^{-1} K at 100 K, which is indicative of complete SCO with a transition temperature ($T_{1/2}$) of 267 K (Fig. S4†). The first-order phase transition was further confirmed by heat capacity measurements over the SCO range with $T_{1/2}$ = 265 K and this was in agreement with the transition temperature obtained from the magnetic data for **1** (Fig. S9†). The entropy and enthalpy changes associated with the spin transition were ΔS = 43.97 (±0.73) J K^{-1} mol^{-1} and ΔH = 11.34 (±0.16) kJ mol^{-1}, respectively, indicating that the thermal-induced SCO is an entropy-driven process. In addition, the temperature-dependent Raman spectra of **1** revealed that a significant increase in the stretching intensity at 2120 cm^{-1} (LS) and a clear decrease at 2075 cm^{-1} (HS) were caused by a further reduction in temperature. The band (2075 cm^{-1}) of the HS state disappeared at 100 K providing further evidence of complete spin transition behavior (Fig. S10†). Similar to Raman spectra, temperature-dependent IR spectra are also very useful to clarify the thermal-induced SCO process. Both the decrease of the HS mode at 2076 cm^{-1} and the increase of the LS mode at 2121 cm^{-1} in the intensity of ν_{NCS^-} stretching bands were caused by decreasing temperature (Fig. S11†), which further confirms the occurrence of thermal-induced SCO behavior.

Temperature-dependent fluorescence emission spectra were also obtained to further elucidate the correlation between fluorescence and SCO from 300 to 10 K. Upon cooling, the emission intensity of the ligand gradually increased as a result of the suppression of thermal fluorescence quenching (Fig. S8†). However, when compared with the free ligand, complex **1** exhibited significantly different temperature-

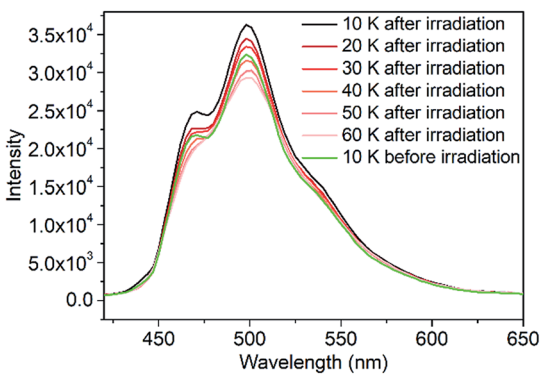

Fig. 2 Thermal variations in the fluorescence emission of **1** after irradiation in the heating mode.

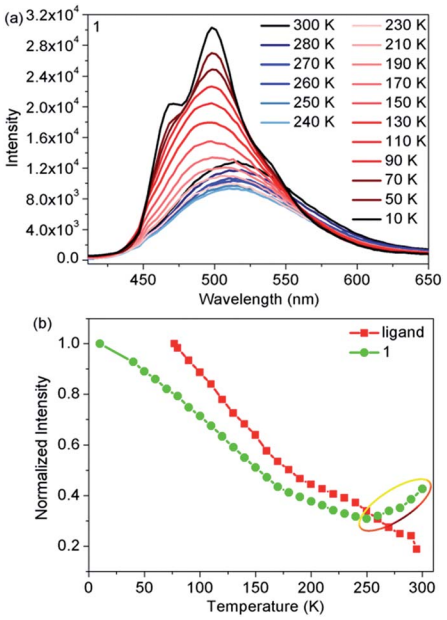

Fig. 3 (a) Temperature-dependent fluorescence emission spectra for complex **1**; (b) normalized maximum fluorescence emission intensity as a function of temperature for the ligand (λ_{em} = 516 nm) and **1** (λ_{em} = 513 nm at 300–170 K and λ_{em} = 498 nm at 160–10 K).

dependent fluorescence emission behavior (Fig. 3a). The emission intensity of **1** initially decreased with decreasing temperature, then reached the lowest value at 250 K. Upon further cooling, the emission intensity started to gradually increase and finally reached a maximum at 10 K (Fig. 3b). In addition, the maximum emission exhibited a marked hypsochromic shift of 15 nm as **1** was cooled from 300 to 100 K. A comparison of the magnetic and fluorescent properties shows that abnormal regions only occurred in the abrupt spin transition process from Fe_{HS}^{II} to Fe_{LS}^{II} ions. Moreover, the emission intensity of the HS state was stronger than that of the LS state in the narrow spin transition temperature range, demonstrating that fluorescence is indeed affected by the spin state of Fe^{II} ions more than the thermal treatment in the spin transition process. The results not only provide direct evidence for the synergy between fluorescence and thermal-induced SCO, but also confirm the earlier conclusion that the photoinduced fluorescence increase in emission intensity was controlled by photoinduced SCO from Fe_{LS}^{II} to Fe_{HS}^{II} ions.

To better understand the modulation mechanism, the variable UV-vis absorption spectra were recorded and they showed that the absorption intensity gradually increased upon cooling (Fig. 4). A new absorption band started to appear at around 700 nm at 260 K and the intensity increased with a lowering of the temperature, which was ascribed to the $^1A_1 \rightarrow {}^1T_1$ transitions of the Fe_{LS}^{II} ion.[38] Furthermore, the time-dependent density functional theory (TD-DFT) calculated UV-vis absorption spectra of complex **1** in its HS and LS states were also obtained to help determine the possible electronic transition processes. The structures of the ground states and the low-lying excited states of the HS and LS complexes were fully optimized and verified using frequency calculations. The optimized LS and HS ground state structures of **1** compared well with their experimental counterparts. A calculated absorption peak at 388 nm for the HS state can be assigned to the intrapyrene $\pi \rightarrow \pi^*$ transition and this is in agreement with the experimentally observed peaks at around 410 nm (Fig. S13†). Another calculated absorption peak at 476 nm was derived from the d(Fe) + π(SCN) $\rightarrow \pi^*$(pyrene) transitions and is ascribed to a metal-to-ligand charge transition (MLCT) and ligand-to-ligand charge

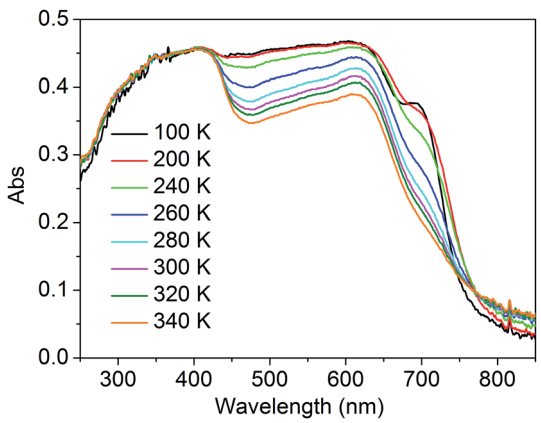

Fig. 4 Temperature-dependent absorption spectra of **1**.

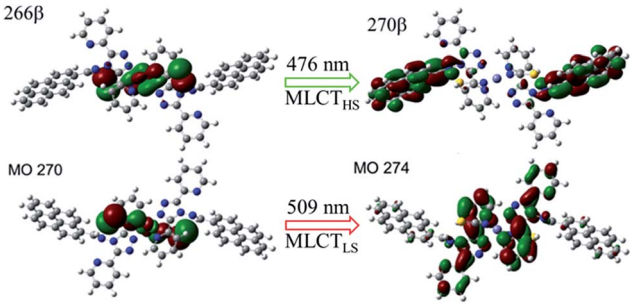

Fig. 5 Characteristic orbitals related to the MLCT transitions of **1** for the HS and LS states.

transition (LLCT). As for the LS state, the calculated peaks centred around 392 and 509 nm. The former mainly arose from the $\pi \rightarrow \pi^*$ excitation within the pyrene groups with a small MLCT contribution, and the latter mainly corresponded to d(Fe) + π(SCN) $\rightarrow \pi^*$(adpt) transitions (Fig. S15†). For the calculated MLCT bands, the charge acceptor is the pyrene group in the HS state, whereas it is mainly the adpt group in the LS state (Fig. 5). This discrepancy likely caused the bathochromic shift (33 nm) of the M_{LS}LCT absorption band in the LS state. Compared with that in the HS state, the fluorescence emission band of the LS state shows opposing hypsochromic shifts (15 nm) (Fig. S16†). These phenomena together lead to an increase in the spectral overlap between M_{LS}LCT absorption and fluorescence emission in the LS state, indicating that the energy level of the M_{LS}LCT excitation closely matches that of the excited state related to the fluorescent ligand. Therefore, the excited state energy of the ligand may be transferred to the Fe_{LS}^{II} ions *via* the resonant energy transfer process, which further leads to quenching of the fluorescence during spin transition from the HS state to the LS state.

In contrast to the LS complex, the HS complex exhibits a small and insignificant spectral overlap between fluorescence emission and M_{HS}LCT absorption. This result further suggests that the energy level of the M_{HS}LCT is slightly higher than the excited energy level of the ligand. Therefore, the excited energy of the ligand cannot be effectively transferred to the Fe_{HS}^{II} center and the fluorescence is only slightly decreased in the HS state. After light irradiation, complex **1** underwent an incomplete light-induced SCO from the LS state to the metastable HS state. The energy transfer process is partly deactivated due to a decrease of the LS species, causing a slight increase in the emission intensity after irradiation. Therefore, fluorescence modulation *via* the LIESST effect is related to the energy transfer between the excited state of the ligand and the energy level of M_{LS}LCT excitation.

Conclusions

In summary, a photoinduced Fe^{II} SCO unit has been coupled with a fluorescent ligand *via* coordination bonds, and the fluorescence emission can be modulated by their synergy. Theoretical and experimental analyses showed that the modulation mechanism arises mainly from the energy transfer from

the excited state of the fluorescent ligand to the MLCT energy level of Fe_{LS}^{II} ions. These findings demonstrate that photoinduced Fe^{II} SCO can serve as a light-responsive unit for coupling with a fluorophore, providing a potential approach for producing switched devices with photoinduced fluorescence.

Conflicts of interest

The authors declare no competing financial interests.

Acknowledgements

This study was partly supported by the NSFC (Grants 21421005, 21322103, 91422302, 21771029, 21373036 and 21573034), the Open Fund of the National Laboratory of Molecular Science (20140116), the Special Program for Applied Research on Super Computation of the NSFC-Guangdong Joint Fund (the second phase) under Grant No. U1501501, and the Chinese Scholarship Council (201706060254). The supercomputer time was supported by the National Supercomputing Center in Guangzhou, China and the High Performance Computing Center at Dalian University of Technology.

Notes and references

1 Z. Hu, B. J. Deibert and J. Li, *Chem. Soc. Rev.*, 2014, **43**, 5815–5840.
2 S. V. Eliseeva and J.-C. G. Bunzli, *Chem. Soc. Rev.*, 2010, **39**, 189–227.
3 K. M. Chan, D. K. Kölmel, S. Wang and E. T. Kool, *Angew. Chem., Int. Ed.*, 2017, **56**, 6497–6501.
4 J. Su, T. Fukaminato, J.-P. Placial, T. Onodera, R. Suzuki, H. Oikawa, A. Brosseau, F. Brisset, R. Pansu, K. Nakatani and R. Métivier, *Angew. Chem., Int. Ed.*, 2016, **55**, 3662–3666.
5 S.-J. Lim, J. Seo and S. Y. Park, *J. Am. Chem. Soc.*, 2006, **128**, 14542–14547.
6 I. Yildiz, E. Deniz and F. M. Raymo, *Chem. Soc. Rev.*, 2009, **38**, 1859–1867.
7 M. Natali and S. Giordani, *Chem. Soc. Rev.*, 2012, **41**, 4010–4029.
8 Y. Hashimoto, T. Nakashima, D. Shimizu and T. Kawai, *Chem. Commun.*, 2016, **52**, 5171–5174.
9 Q. Zhang, H. Sun, X. Wang, X. Hao and S. An, *ACS Appl. Mater. Interfaces*, 2015, **7**, 25289–25297.
10 I. L. Medintz, S. A. Trammell, H. Mattoussi and J. M. Mauro, *J. Am. Chem. Soc.*, 2004, **126**, 30–31.
11 R. Pardo, M. Zayat and D. Levy, *Chem. Soc. Rev.*, 2011, **40**, 672–687.
12 S. Ishida, T. Fukaminato, D. Kitagawa, S. Kobatake, S. Kim, T. Ogata and S. Kurihara, *Chem. Commun.*, 2017, **53**, 8268–8271.
13 K. Jeong, S. Park, Y.-D. Lee, C.-K. Lim, J. Kim, B. H. Chung, I. C. Kwon, C. R. Park and S. Kim, *Adv. Mater.*, 2013, **25**, 5574–5580.
14 J. W. Chung, S.-J. Yoon, S.-J. Lim, B.-K. An and S. Y. Park, *Angew. Chem., Int. Ed.*, 2009, **48**, 7030–7034.
15 K. A. Green, M. P. Cifuentes, T. C. Corkery, M. Samoc and M. G. Humphrey, *Angew. Chem., Int. Ed.*, 2009, **48**, 7867–7870.
16 S.-J. Lim, B.-K. An, S. D. Jung, M.-A. Chung and S. Y. Park, *Angew. Chem., Int. Ed.*, 2004, **43**, 6346–6350.
17 J. Moreno, M. Gerecke, L. Grubert, S. A. Kovalenko and S. Hecht, *Angew. Chem., Int. Ed.*, 2016, **55**, 1544–1547.
18 S. Castellanos, A. Goulet-Hanssens, F. Zhao, A. Dikhtiarenko, A. Pustovarenko, S. Hecht, J. Gascon, F. Kapteijn and D. Bléger, *Chem.–Eur. J.*, 2016, **22**, 746–752.
19 C. Knie, M. Utecht, F. Zhao, H. Kulla, S. Kovalenko, A. M. Brouwer, P. Saalfrank, S. Hecht and D. Bléger, *Chem.–Eur. J.*, 2014, **20**, 16492–16501.
20 F. M. Raymo and M. Tomasulo, *Chem. Soc. Rev.*, 2005, **34**, 327–336.
21 A. Bousseksou, G. Molnár, J. A. Real and K. Tanaka, *Coord. Chem. Rev.*, 2007, **251**, 1822–1833.
22 S. Ohkoshi, S. Takano, K. Imoto, M. Yoshikiyo, A. Namai and H. Tokoro, *Nat. Photonics*, 2013, **8**, 65–71.
23 D.-P. Dong, T. Liu, S. Kanegawa, S. Kang, O. Sato, C. He and C.-Y. Duan, *Angew. Chem., Int. Ed.*, 2012, **51**, 5119–5123.
24 M. Engeser, L. Fabbrizzi, M. Licchelli and D. Sacchi, *Chem. Commun.*, 1999, 1191–1192.
25 M. Masaki, I. Hikaru and T. Hiroyuki, *Chem. Lett.*, 2008, **37**, 374–375.
26 L. Salmon, G. Molnar, D. Zitouni, C. Quintero, C. Bergaud, J.-C. Micheau and A. Bousseksou, *J. Mater. Chem.*, 2010, **20**, 5499–5503.
27 S. Titos-Padilla, J. M. Herrera, X.-W. Chen, J. J. Delgado and E. Colacio, *Angew. Chem., Int. Ed.*, 2011, **50**, 3290–3293.
28 C. M. Quintero, I. y. A. Gural'skiy, L. Salmon, G. Molnar, C. Bergaud and A. Bousseksou, *J. Mater. Chem.*, 2012, **22**, 3745–3751.
29 C.-F. Wang, R.-F. Li, X.-Y. Chen, R.-J. Wei, L.-S. Zheng and J. Tao, *Angew. Chem., Int. Ed.*, 2015, **54**, 1574–1577.
30 C.-F. Wang, M.-J. Sun, Q.-J. Guo, Z.-X. Cao, L.-S. Zheng and J. Tao, *Chem. Commun.*, 2016, **52**, 14322–14325.
31 Y. Garcia, F. Robert, A. D. Naik, G. Zhou, B. Tinant, K. Robeyns, S. Michotte and L. Piraux, *J. Am. Chem. Soc.*, 2011, **133**, 15850–15853.
32 M. Estrader, J. Salinas Uber, L. A. Barrios, J. Garcia, P. Lloyd-Williams, O. Roubeau, S. J. Teat and G. Aromi, *Angew. Chem., Int. Ed.*, 2017, **56**, 15622–15627.
33 Y. Jiao, J. Zhu, Y. Guo, W. He and Z. Guo, *J. Mater. Chem. C*, 2017, **5**, 5214–5222.
34 B. Schäfer, T. Bauer, I. Faus, J. A. Wolny, F. Dahms, O. Fuhr, S. Lebedkin, H. C. Wille, K. Schlage, K. Chevalier, F. Rupp, R. Diller, V. Schunemann, M. M. Kappes and M. Ruben, *Dalton Trans.*, 2017, **46**, 2289–2302.
35 I.-R. Jeon, C. Mathoniere, R. Clerac, M. Rouzieres, O. Jeannin, E. Trzop, E. Collet and M. Fourmigue, *Chem. Commun.*, 2017, **53**, 10283–10286.
36 C. Mathonière, H.-J. Lin, D. Siretanu, R. Clérac and J. M. Smith, *J. Am. Chem. Soc.*, 2013, **135**, 19083–19086.
37 H. Phan, S. M. Benjamin, E. Steven, J. S. Brooks and M. Shatruk, *Angew. Chem., Int. Ed.*, 2015, **54**, 823–827.

38 S. Ohkoshi, K. Imoto, Y. Tsunobuchi, S. Takano and H. Tokoro, *Nat. Chem.*, 2011, **3**, 564–569.
39 J.-F. Létard, *J. Mater. Chem.*, 2006, **16**, 2550–2559.
40 S. Decurtins, P. Gütlich, C. P. Köhler and H. Spiering, *Chem. Phys. Lett.*, 1984, **105**, 1–4.
41 A. Hauser, *Chem. Phys. Lett.*, 1986, **124**, 543–548.
42 L. J. Kershaw Cook, H. J. Shepherd, T. P. Comyn, C. Baldé, O. Cespedes, G. Chastanet and M. A. Halcrow, *Chem.–Eur. J.*, 2015, **21**, 4805–4816.
43 C.-F. Sheu, S.-M. Chen, S.-C. Wang, G.-H. Lee, Y.-H. Liu and Y. Wang, *Chem. Commun.*, 2009, 7512–7514.
44 C.-H. Shih, C.-F. Sheu, K. Kato, K. Sugimoto, J. Kim, Y. Wang and M. Takata, *Dalton Trans.*, 2010, **39**, 9794–9800.
45 R. W. Hogue, H. L. C. Feltham, R. G. Miller and S. Brooker, *Inorg. Chem.*, 2016, **55**, 4152–4165.
46 J.-L. Wang, Q. Liu, Y.-S. Meng, H. Zheng, H.-L. Zhu, Q. Shi and T. Liu, *Inorg. Chem.*, 2017, **56**, 10674–10680.
47 W. Phonsri, P. Harding, L. Liu, S. G. Telfer, K. S. Murray, B. Moubaraki, T. M. Ross, G. N. L. Jameson and D. J. Harding, *Chem. Sci.*, 2017, **8**, 3949–3959.